Ph.D. Dissertation of Medicine

Spatial Distribution of Myeloid-derived Suppressor Cell Subtypes Reveals Its Clinical and Prognostic Roles in Advanced Gastric Cancer

진행성 위암에서 다중면역화학염색을 통해 판별된 골수유래 면역억제세포의 공간적 분포와 아형에 따른 임상적 의미 및 예후와의 연관성에 대하여

August 2021

Graduate School of Medicine
Seoul National University
Pathology Major

김영훈

Spatial Distribution of Myeloid-derived Suppressor Cell Subtypes Reveals Its Clinical and Prognostic Roles in Advanced Gastric Cancer

지도 교수 강경훈

Submitting a Ph.D. Dissertation of Medicine

April 2021

Graduate School of Medicine
Seoul National University
Pathology Major
김 영 훈

Confirming the Ph.D. Dissertation written by
김 영 훈
July 2021

Chair _____
Vice Chair _____
Examiner _____
Examiner _____
Examiner _____

Abstract

Introduction: Myeloid-derived suppressor cells (MDSCs) are heterogenous population of immature myeloid cells that are found in pathological conditions including cancer. These cells are renowned to play a vital role within the tumor microenvironment (TME), but information about their distribution and impact on clinical features are not reported in gastric cancer (GC).

Materials and methods: A respective study included 59 patients with advanced GC. Tissue microarray and multiplex immunohistochemistry was used to assess the immune cell components of the TME which includes subtypes of MDSC and T cells. Clinicopathological characteristics including prognosis were correlated with these immune cells.

Results: PMN-MDSC was most abundant followed by M-MDSC. MSS/EBV-negative GCs were T cell low even when MDSC were high unlike EBV-positive and MSI-high GCs. PD-L1 expression was more frequent in M-MDSC. All MDSC subsets were located close to tumor cells as was CD8+ T cells

Conclusion: MDSCs resides in a distinct niche within the TME of GC. These features pose MDSC as a potential target for improved treatment.

Keyword: Myeloid-derived suppressor cell, advanced gastric cancer, tumor microenvironment, multiplex immunohistochemistry, prognosis, immune system

Student Number: 2012-21737

Contents

List of Tables

List of Figures

INTRODUCTION

Gastric cancer (GC) is the one of the most common malignancy and third leading cause of cancer mortality worldwide (1, 2) with most of its patients occur at Eastern Asia including Korea (3). GC is a heterogenous disease with diverse molecular phenotype. These include genome-wide genetic and epigenetic alterations including DNA mutation, copy number variation, aberrant DNA methylation, histone modification, presence of noncoding RNA, and RNA editing (4). Moreover, it has been proven that the tumor microenvironment (TME) also plays a crucial role in tumor initiation, tumor progression, and metastasis (5). However, the tumor immune milieu, which affect tumorigenesis and treatment plans has not been fully elucidated.

Myeloid-derived suppressor cells (MDSCs) are important component of the TME. They are a heterogeneous population of immature myeloid cells derived from myeloid progenitor cells (6), and are considered as immature precursors of dendritic cells, granulocytes, and macrophages (7). Moreover, MDSCs are a result of aberrant sustained myelopoiesis otherwise resolved after recovery from injury or inflammation. MDSCs are observed in chronic inflammation, autoimmune disease, and cancer and have a pathologic activation that are different from their mature and terminally differentiated myeloid cell counterpart (6).

Detecting subsets of MDSC has been complex in human cancer (8). This is in part due to the fact that MDSCs are composed of a heterogenous myeloid cells including polymorphonuclear-MDSC (PMN-MDSC), monocytic-MDSC(M-MDSC), and early stage MDSC (eMDSC). PMN-MDSC (or granulocyte-MDSC) represent the most abundant population of MDSC in human and in mice (9). These cells suppress the function of other immune cells and as well as promote tumor progression and metastasis with non-immune mechanisms (10, 11). M-MDSC is strongly associated with macrophage in lineage and is considered to have more potent than PMN-MDSC despite being less in numbers (12), although conflicting evidence also exists both

in potency and in number (13, 14). These cells suppress T cells via up-regulation of NO and arginase, production of immune suppressive cytokines, and other non-contact mechanism. eMDSC is an early precursor MDSC that lack markers for both PMN-MDSC and M-MDSC. However, its functional distinction from PMN-MDSC and M-MDSC are still questionable (13).

The other part of the complexity comes from the fact that characterization of MDSC has not been perplexed and not been standardized. To detect human MDSCs, at least one common myeloid cell marker (CD33, CD11b or CD66) showed be paired with CD14, CD15, HLA-DR and other MDSC-associated markers. Due to the complexity in nomenclature and detection markers, most studies involving MDSC has been limited to single cell detection methods including flow cytometry and single cell RNA sequencing (Table 1). However, these techniques dissolve the whole tissue into single cells and do not preserve spatial information.

In this study, PMN-MDSC, M-MDSC, and eMDSC were identified and characterized in advanced GC specimen via multiplex immunohistochemistry (IHC). This allowed us to observe distance between tumor cells and immune cells as well as determine the density of each immune cell as TME gets further from the nearest tumor cell. We believe these finding will provide essential clues in deciphering the role of MDSC in TME.

Table 1. Previous studies on detecting MDSCs.

Tumor	Markers	Method	Year
Colorectal	CD45+CD11b+CD33+	Flow cytometry	2013
Colorectal	HLA-DR-CD33+CD11bhiCD14-CD18+CD1a+	Flow cytometry	2012
Breast	CD45+CD33+CD13+CD14-CD15-	Flow cytometry	2013
HCC	CD14hiHLA-DRloCD11bhiCD11chiCD33hi	Flow cytometry	2008
Ovarian	Lin-1-CD45+CD33+HLA-DRintCD15-CD16lo	Flow cytometry	2011
Pancreas	CD15+CD33+CD11b+	Flow cytometry	2012
Lung	CD33+(with PD-L1/CD4/CD8)	Multiplex IHC	2018

MATERIALS AND METHODS

Patient samples and molecular phenotypes

Formalin-fixed paraffin-embedded (FFPE) samples of advanced gastric cancers from 59 patients who underwent surgery at Seoul National University Hospital in 2018 was collected. The resected samples were primary tumors that were not exposed to chemotherapy and/or radiotherapy before the surgery. Forty-two patients were diagnosed with adenocarcinoma and 17 patients were poorly cohesive carcinoma. Tumor stage was classified according to the American Joint Committee on Cancer system (7^{th} edition). Ten patients were stage I, 18 patients were stage II, three patients were stage III, and four patients were stage IV. This study was approved by institutional review board, which waived requirement to obtain informed consent.

Microsatellite (MSI) status was determined by utilizing five-marker scoring panel, namely *BAT25*, *BAT26*, *D2S123*, *D5S345*, and *D17250.* MSI-high was defined when ≥ 40% of markers showed instability, MSI-low was defined as presence of one instable marker, and microsatellite stable (MSS) was defined as no marker with instability. Epstein-Barr virus (EBV) infection status was detected by *EBER1* silver in situ hybridization as described previously (15). According to these findings, AGCs were categorize as EBV-positive, MSI-high, or EBV-negative/MSS.

Multiplex IHC with tissue microarray block

Through histological examination by pathologist (YK), a 2.0-mm diameter tumor samples from each patients' FFPE block were extracted and rearranged into a single tissue microarray (TMA) block using a trephine apparatus. A pair of 4-μm section was obtained from the TMA block and mounted to glass slides to perform multiplex IHC (Figure 1a). Sections were deparaffined with xylene and serially hydrated with gradually decreasing concentration of alcohols and eventually distilled water. Following antigen retrieval and cooling in room temperature, blocking was applied to each section with

methanol based 0.3% hydrogen peroxide and 4% non-fat skimmed milk, sequentially. A different set of primary antibodies were applied to each section. Antibodies for MDSC included anti-CD11b (clone EP1345Y, 1:100, Abcam, Cambridge, UK), anti-CD33 (clone 6C5/2, 1:100, Abcam), anti-CD14 (R&D Systems, Minneapolis, MN, USA), anti-CD15 (clone Carb-3, Dako, Glostrup, Denmark), anti-CD16 (SP175, 1:100, Abcam), anti-HLA-DR (1:500, Santa Cruz Biotechnology, Santa Cruz, CA, USA), anti-PD-L1 (1:30, Cell Signaling, Beverly, MA, USA), and cytokeratin antibodies (clone AE1/AE3, 1:300, Dako) (Figure 1b). Antibodies to detect T cells included anti-CD3 (1:300, Dako), anti-CD8 (clone SP57, Roche, Basel, Switzerland), anti-FOXP3 (clone 236A/E7, 1:50, Abcam), anti-CD45RO (clone UCHL1, Cell Marque, Rocklin, CA), anti-PD-1 (clone D4W2J, Cell Signaling), anti-PD-L1, and anti-cytokeratin antibodies (Figure 1c). Only one primary antibody was applied in a single cycle. ImmPACT NovaRED (Vector Laboratories, Burlingame, CA, USA) was used to catalyze peroxidase substrate from the secondary antibody. Slides were stained with hematoxylin for counterstaining. The slide sections were coverslipped with cover glass and scanned by Aperio AT2 scanner (Leica Biosystems, New Castle, UK), which created a file of a virtual slide for each staining. To strip the antibodies, glass slides containing the TMA were soaked in stripping solution (20% SDS, 0.5M Tris HCl buffer, and 2-Mercaptoethanol) and heated in 56°C for 40 min. Slides were microwaved at low power to get more stripping effects. A new cycle was restarted from the antigen retrieval step followed by attaching a new primary antibody (Figure 1a).

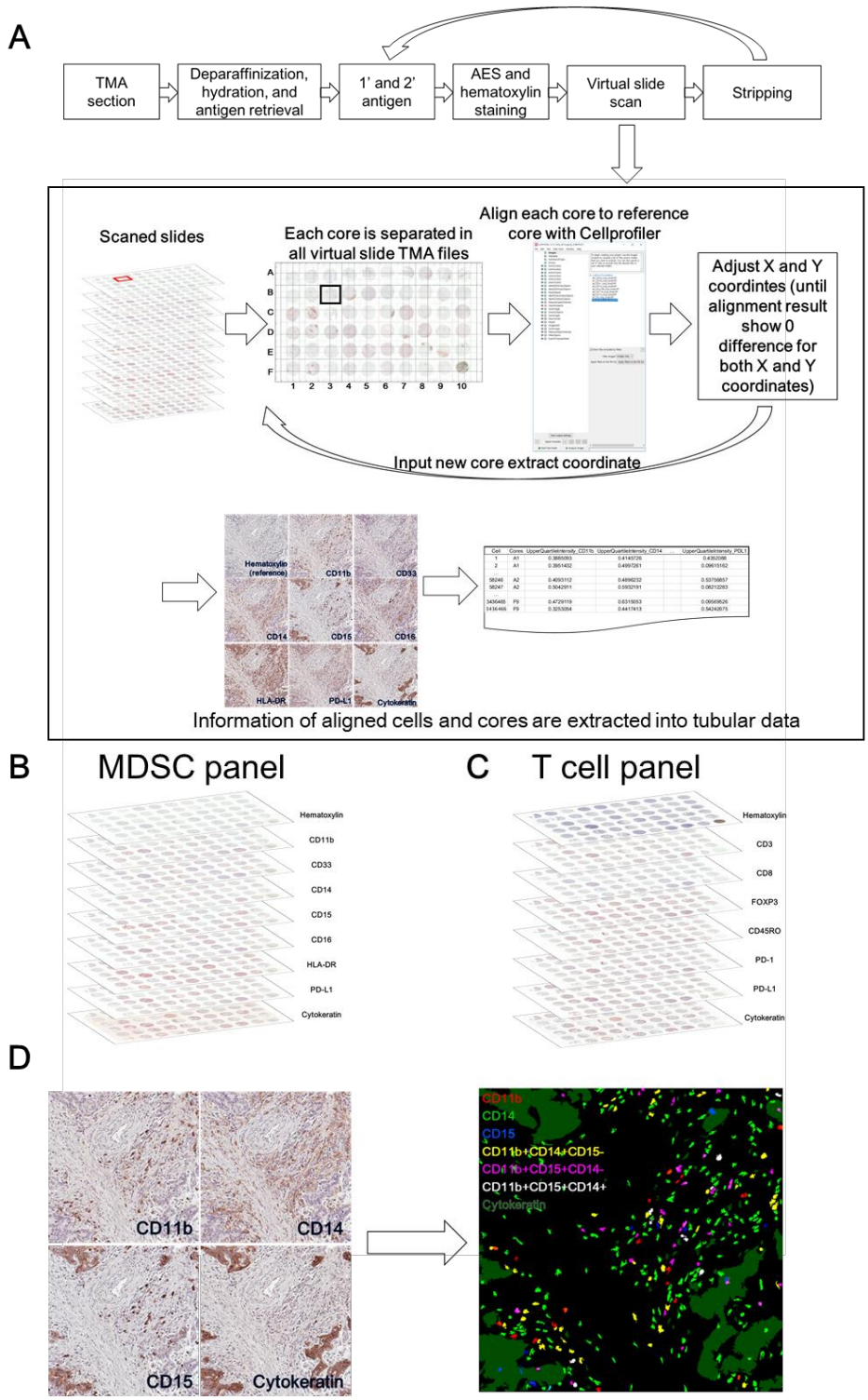

Figure 1. Process of multiplex IHC. A, Brief flow chart; B, multiplex virtual slides to identify subsets of MDSC; C, multiplex virtual slides to identify subsets of T cells; D, Pseudocolor of virtual slides for MDSC detection

Core separation, alignment, determining cutoff value, and data analysis

Each TMA core was separated as an 8,000 x 8,000 pixel TIFF image (corresponding to 2 x 2 mm^2) via QuPath (16) and Aperio ImageScope (Lecia Biosystems). In detail, TMA dearrayer function in QuPath provided central coordinates of each core (X and Y coordinates) and Apero ImageScope extracted the image according to the provided coordinates without losing image quality. A total of 1,003 image files were generated (531 from MDSC panels and 472 from T cell panels). CellProfiler was used for further image analysis (17). Alignment of images from the same slide and same core (which includes markers from the identical panel) was based on fast normalized cross-correlation and evaluated locations of individual cell nucleus identified from slides with only hematoxylin channel (upper most slides of Figure 1b and 1c). The alignment process was repeated until each core showed no difference between X and Y coordinates across all markers in the same panel (Figure 1a). Positive cells were defined as cells showing upper quartile intensity greater than the threshold level. Features from each core were extracted in a tubular data format. The variables include cellular features such as various nuclear features, intensity of each staining, cell location, and distance from closest tumor cell, as well as core-associated features such as overall tissue area, tumor area, and stromal area. Tumor cells were detected by cytokeratin expression. Cutoff value of each protein expression was determined by matching visually positive cells to pseudocolor image generated based on upper quantile intensity of cells (exemplified in Figure 1d).

Statistical methods

Statistical analysis was carried out with R program (version 3.5.2). Correlation between immune cells were analyzed via R package corrplot. Hierarchical clustering and heatmap construction was performed with gplots package. Difference between two variables was calculated by using the Mann-Whitney U test.

Spearman correlation showed the correlation between cell densities.

RESULTS

Immune cell type detection and cellular proportions

Myeloid and T cells were verified according to expression of each marker. Markers used to identify cells are summarized in Table 2. Cells within MDSC panel were categorized by phenotypes suggested from previous studies (4,5). Overall number of cells determined by hematoxylin-stained nuclear count was 599,579 in MDSC panel TMA cores (average of 10,162 cell per core). As for the whole tissue core, 12,686 cells (2.12%) were considered as MDSC, which was roughly one third of 39,194 CD11b+ cells. These cells were predominantly PMN-MDSC (92.72% of total MDSC) followed by M-MDSC (6.39% of total MDSC) and eMDSC (0.89% of total MDSC) (Figure 2a). Intratumoral and stromal proportion of total MDSC and its subsets were also investigated. In PMN-MNDS population, 27.52% and 72.48% of cells were located in intraturmoral and stromal areas, respectively (Figure 2b). In M-MDSC population, the distribution for intratumoral and stromal area was 13.93% and 86.67%, respectivley, and for eMDSC, this distrubtion was 14.16% and 85.84%, respectively (Figure 2b). For T cell panel, a total of 609,851 cells were evaluated. Proportion of each T cell subset (Figure 2c) and its relative proportions (Figure 2d) in intratumoral and stromal areas were addressed according to T cell markers (Table 2).

Table 2. T cell, TAM and MDSC markers

T lymphocyte lineage	**Subset markers**				
All T lymphocytes	$CD3^+$				
$CD8^+$ T lymphocyte (CD8+T)	$CD3^+$	$CD8^+$			
Helper T cell (TH)	$CD3^+$	$CD8^-$	$FOXP3^-$		
Regulatory T cell (Treg)	$CD3^+$	$CD8^-$	$FOXP3^+$		
Additional T cell subsets	**Subset markers**				
$PD\text{-}L1^+$	$PD\text{-}L1^+$	T cells			
$PD\text{-}1^+$	$PD\text{-}1^+$	T cells			
$PD\text{-}L1^+/PD\text{-}1^+$	$PD\text{-}L1^+$	$PD\text{-}1^+$	T cells		
memory/activated subset	$CD45RO^+$	T cells			
TAM and MDSC lineage	**Subset markers**				
Macrophage	$CD11b^+$	$CD14^+$	HLA-DR^+		
PMN-MDSC	$CD11b^+$	$CD15^+$	$CD14^-$	$HLA\text{-}DR^{low/-}$	
M-MDSC	$CD11b^+$	$CD14^+$	$CD15^-$	$HLA\text{-}DR^{low/-}$	
eMDSC	$CD11b^+$	$CD33^+$	$CD15^-$	$CD14^-$	HLA-$DR^{low/-}$
Additional MDSC subsets	**Subset markers**				
$PD\text{-}L1^+$	$PD\text{-}L1^+$	MDSCs			
$CD16^+$	$CD16^+$	MDSCs			

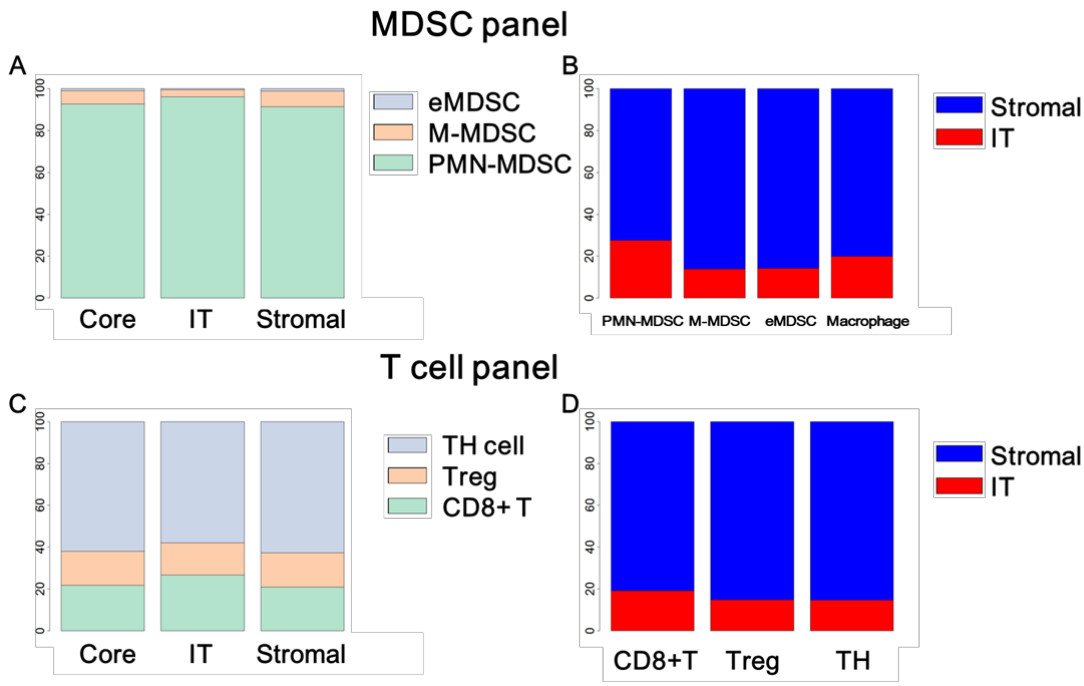

Figure 2. MDSC and T cell proportion in intratumoral and stromal regions. A, Subsets of MDSC proportion in each region; B, Regional proportion of MDSCs; C, Subsets of T cell proportion in each region; D, Regional proportion in T cells.

Core; region of IT and stromal combined, IT: intratumoral

Correlation between immune cell subsets densities

Correlation between each immune cell densities were examined. A strong positive correlation was shown between PMN-MDSC and eMDSC (Figures 3a to 3c). Although a positive correlation between overall myeloid cell (represented as CD11b+) and T cells were observed, significant correlation between MDSC and T cells were limited to an inverted correlation M-MDSC and regulatory T cells in total and stromal areas (Figures 3a and 3b). Future more, M-MDSC showed a positive correlation with NK cell marker CD57 while PMN-MDSC and M-MDSC showed positive correlation with memory T cells (not shown in figure).

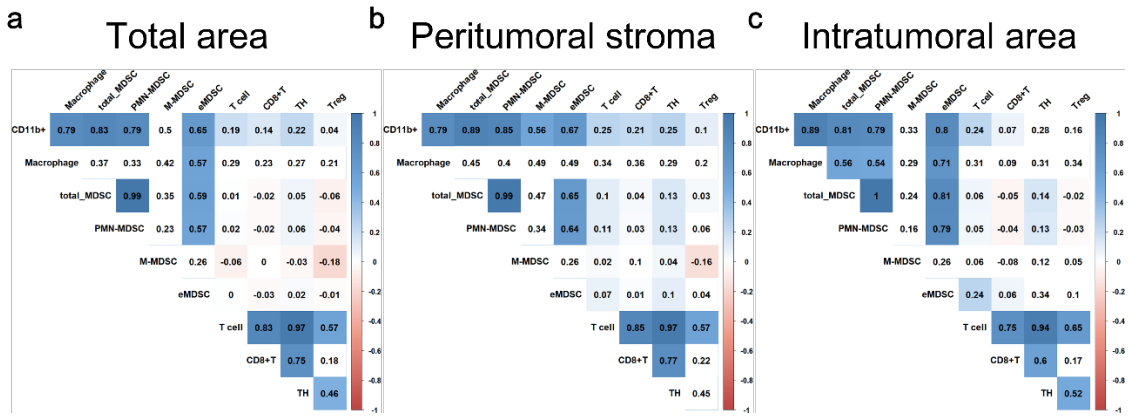

Figure 3. Correlation between myeloid and T cell subsets. A, Correlation in total area; B, Correlation in stromal area; C, Correlation in intratumoral area

MDSC and Clinicopathological features of GC

Unsupervised clustering of MDSC and TIL densities were analyzed as immune cells of intratumoral and stromal regions considered as a separate entity (Figure 4). All specimens were categorized as myeloid cell rich, lymphocyte rich, or immune cell poor. Most EBV-postive and MSI-high cancers were considered as myeloid cell rich, while only a single MSI-high GC was considered as immune cell poor. pTNM staging did not show significant correlation with immune cell clustering.

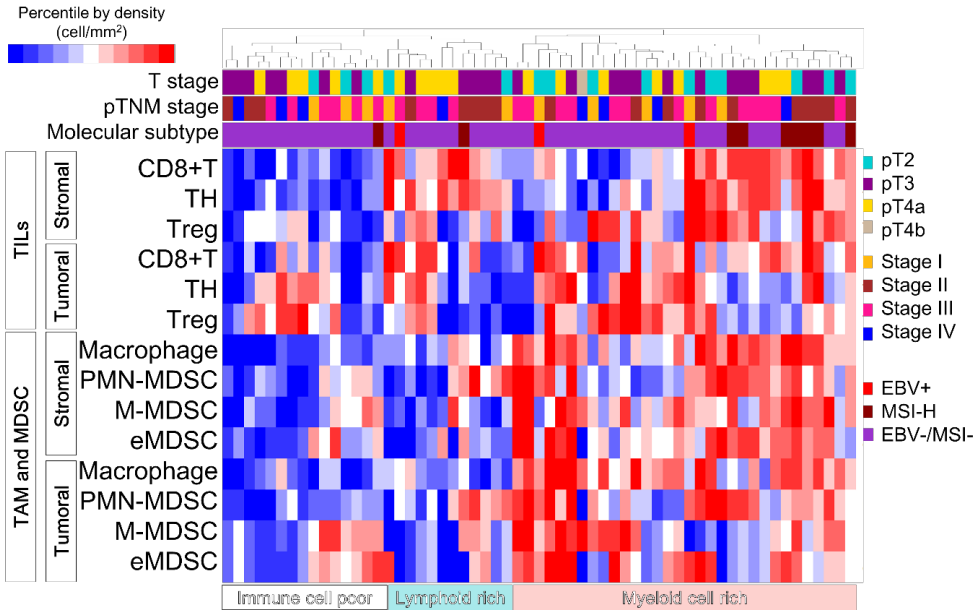

Figure 4. Unsupervised clustering of MDSC and T cell subset densities.

CD16, CD45RO, PD-L1, and PD-1 expression in immune cells

Additional MDSC and T cell subsets were explored. CD16 expression in M-MDSC was high than that of PMN-MDSC (Figures 5a and 5b) but no difference were observed between CD16 expression of intratumoral and stromal regions. CD45RO expression was higher in regulatory and cytotoxic T cells compared with that of helper T cell (Figure 5c). M-MDSC was the MDSC to show highest PD-L1 expression while help T cell showed the lowest PD-L1 expression among the T cell subsets (Figure 5d and 5e). CD8+ T cells showed highest PD-1 expression and PD-L1/PD-1 co-expression followed by regulatory T cells (Figure 5F and 5I). CD16+ PMN- and M-MDSC did not show any significant difference in PD-L1 expression compared with its CD16- counterpart (Figures 5g and 5h).

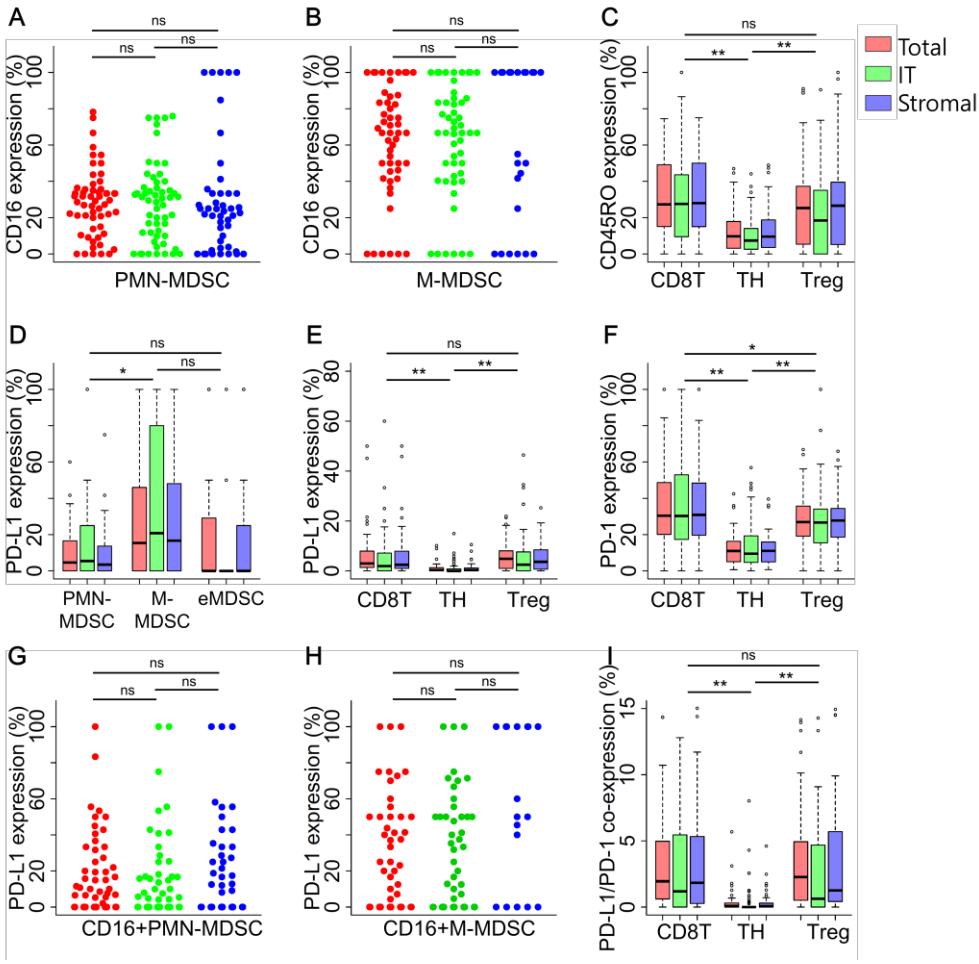

Figure 5. Additional expression in MDSCs and T cells. A, CD16 expression in PMN-MDSC; B, CD16 expression in M-MDSC; C, CD45RO expression in T cells; D, PD-L1 expression in MDSCs; E, PD-L1 expression in T cells; F,PD-1 expression in T cells; G, PD-L1 expression in CD16+ PMN-MDSC; H, PD-L1 expression in CD16+ M-MDSC; I, PD-L1/PD-1 co-expression in T cells.

Immune cell distance from tumor cells

We observed the distance of each MDSC and T cell from the closet tumor cell. Within the myleoid cells, all three MDSCs were closer to tumor cell compared with macrophages (Figure 6a). eMDSC showed a shorter distance with tumor cells compared with PMN-MDSC. Among T cells, CD8+ T cells were closest to tumor cells and regulatory T cells were the furthest (Figure 6b). Interestingly, CD8+ T cells were closer to tumor cells even than memory T cells, which included portions of CD8+ T cells.

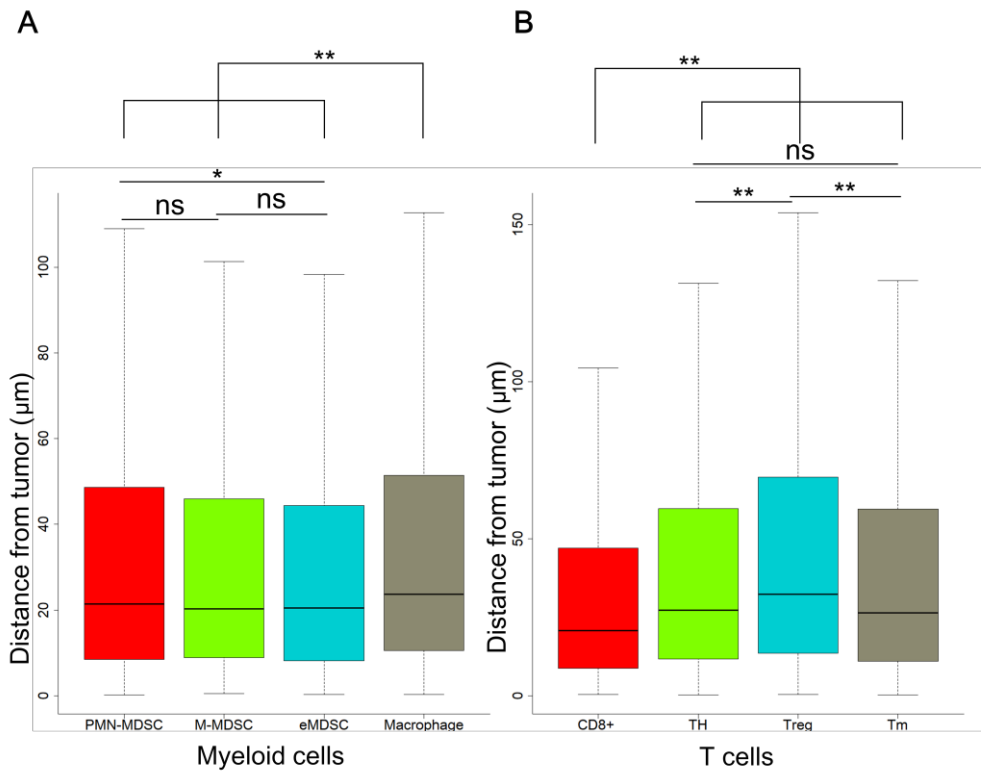

Figure 6. Distance between immune cells and the closest tumor cell. A, distance between tumor cells and myeloid cells; B, distance between tumor cells and T cells.

Prognostic significane of MDSCs

We examined the density of each MDSC subset and patient survival. In Kaplan-Meier analysis with log-rank test, PMN-MDSC and M-MDSC were not associated with prognosis (Figures 7b and 7d). High CD16+ PMN-MDSC was associated with favorable overall survival (Figure 7a) but CD16+ M-MDSC did not show such relationship with survival.

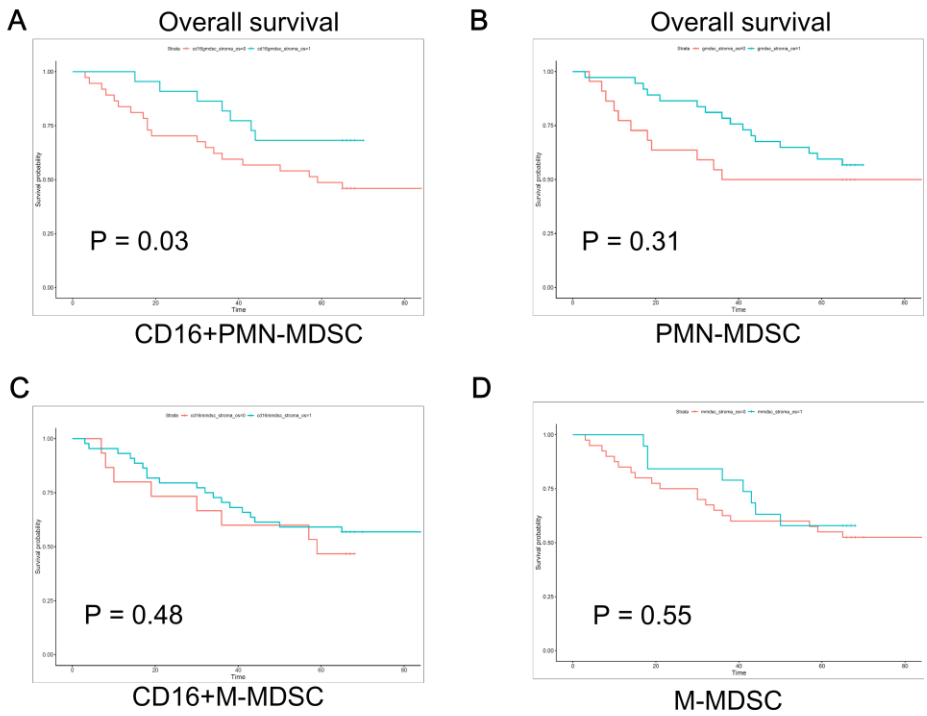

Figure 7. Overall survival of MDSCs. A, CD16+ PMN-MDSC; B, PMN-MDSC; C, CD16+ M-MDSC; D, M-MDSC

DISCUSSION

In our study, we identified distinct population of MDSC in advanced GC with FFPE blocks and multiplex IHC. PMN-MDSCs were most abundant followed by M-MDSCs regardless of intratumoral or stromal region. eMDSCs were sparse in all regions. Despite of the inhibitory role of MDSCs towards T cells, correlation between MDSC and T cell densities were not significant with the the exception of weak inverted correlation between M-MDSC and regulatory T cells (Figure 3). These findings suggest that the suppressive mechanism of MDSC may not be limited to T cell recruitment but more towards functional dysregulation of T cells, as previously articles has insisted (18).

Unsupervised clustering revealed that most EBV-positive and MSI-high GC are associated with high T cells as well as high MDSCs while MSS/EBV-negative GC showed relatively lower T cell densities even when MDSC densities were high. Additional subset analysis for MDSCs and T cells determined that M-MDSC containing higher PD-L1 expression than PMN-MDSC, which may explain how M-MDSC are more potent in activity despite having a smaller number. However, expression difference between CD16 and PD-L1 in intratumoral and stromal regions were negligible.

A defining advantage of multiplex IHC over other single cell analysis techniques would be the ability to preserve spatial information within the specimen. Our findings show that compared with total myeloid cells (defined as CD11b+) or macrophage populations, MDSC were located much closer to tumor cells although the distance between tumor cells and three subtypes of MDSC were not distinct. Recently, multiplex IHC revealed that M2 macrophages are further from tumor cells while macrophages closer to tumor cells are more likely M1 macrophages (19). Since M2 macrophages are also known to have immune suppressive potential, it is likely that MDSC and M2 macrophages play a distinct role in immunosuppression starting by difference in niche within the TME. Among the T cells, CD8+ T cells were closer to tumor cells than any

other T cell population. Since CD8+ T cell also show high PD-1 expression, It is likely that MDSC and CD8+ T cells directly interact near the tumor cell while macrophages interact more frequently with other T cell population further from the tumor cell.

Discovering the characteristic of MDSC and its clinical impact could lead to increased treatment effect on cancer. Nevertheless, depletion, blockage, inhibition, and differentiation of MDSC has been proposed as treatment as well as combining MDSC-targeted treatment with PD-1 inhibitory immunotherapy (20). However, defining MDSCs to target may not be an easy task. For example, high expression level of CD84 were identified in PMN-MDSC and M-MDSC of several tumors (21, 22) but not detected in other tumors (9). Moreover, our data suggests that distance between tumor cell and immune cells in GC could be different from colorectal cancer, which was suggested in a recent study (23). These discrepancies suggest that expression pattern of MDSC could be tumor specific.

There are some limitations to our study. Due to the complexity of marker, our sample size was relatively small. Unlike single cell RNA sequencing, we could not investigate additional potential markers of MDSC including Arg1, Lox1, NOS2, and S100A9. We should overcome these shortcomings in the following studies.

We have identified the characteristic and distribution of MDSC. As far as our knowledge, this is the first study to use such thorough markers to analyze MDSC in advanced GC. Our studies show that MDSC possess a distinct niche which interacts with T cells near the tumor cells within the TME. These findings pose MDSC as a potential therapeutic target that could affect tumor progression and development greatly.

References

1. Machlowska J, Baj J, Sitarz M, Maciejewski R, Sitarz R. Gastric Cancer: Epidemiology, Risk Factors, Classification, Genomic Characteristics and Treatment Strategies. Int J Mol Sci. 2020;21(11). doi: 10.3390/ijms21114012. PubMed PMID: 32512697; PubMed Central PMCID: PMC7312039.
2. Sung H, Ferlay J, Siegel RL, Laversanne M, Soerjomataram I, Jemal A, et al. Global Cancer Statistics 2020: GLOBOCAN Estimates of Incidence and Mortality Worldwide for 36 Cancers in 185 Countries. CA Cancer J Clin. 2021;71(3):209-49. doi: 10.3322/caac.21660. PubMed PMID: 33538338.
3. Ang TL, Fock KM. Clinical epidemiology of gastric cancer. Singapore Med J. 2014;55(12):621-8. doi: 10.11622/smedj.2014174. PubMed PMID: 25630323; PubMed Central PMCID: PMC4291998.
4. Padmanabhan N, Ushijima T, Tan P. How to stomach an epigenetic insult: the gastric cancer epigenome. Nat Rev Gastroenterol Hepatol. 2017;14(8):467-78. doi: 10.1038/nrgastro.2017.53. PubMed PMID: 28513632.
5. Wang M, Zhao J, Zhang L, Wei F, Lian Y, Wu Y, et al. Role of tumor microenvironment in tumorigenesis. J Cancer. 2017;8(5):761-73. doi: 10.7150/jca.17648. PubMed PMID: 28382138; PubMed Central PMCID: PMC5381164.
6. Bronte V, Brandau S, Chen SH, Colombo MP, Frey AB, Greten TF, et al. Recommendations for myeloid-derived suppressor cell nomenclature and characterization standards. Nat Commun. 2016;7:12150. Epub 2016/07/07. doi: 10.1038/ncomms12150. PubMed PMID: 27381735; PubMed Central PMCID: PMC4935811.
7. Gabrilovich DI, Nagaraj S. Myeloid-derived suppressor cells as regulators of the immune system. Nat Rev Immunol. 2009;9(3):162-74. doi: 10.1038/nri2506. PubMed PMID: 19197294; PubMed Central PMCID: PMC2828349.
8. Veglia F, Hashimoto A, Dweep H, Sanseviero E, De Leo A, Tcyganov E, et al. Analysis of classical neutrophils and polymorphonuclear myeloid-derived suppressor cells in cancer patients and tumor-bearing mice. J Exp Med. 2021;218(4). doi: 10.1084/jem.20201803. PubMed PMID: 33566112; PubMed Central PMCID: PMC7879582
9. Zhou J, Nefedova Y, Lei A, Gabrilovich D. Neutrophils and PMN-MDSC: Their biological role and interaction with stromal cells. Semin Immunol. 2018;35:19-28. doi: 10.1016/j.smim.2017.12.004. PubMed PMID: 29254756; PubMed Central PMCID: PMC5866202.

10. Condamine T, Ramachandran I, Youn JI, Gabrilovich DI. Regulation of tumor metastasis by myeloid-derived suppressor cells. Annu Rev Med. 2015;66:97-110. doi: 10.1146/annurev-med-051013-052304. PubMed PMID: 25341012; PubMed Central PMCID: PMC4324727.
11. Veglia F, Perego M, Gabrilovich D. Myeloid-derived suppressor cells coming of age. Nat Immunol. 2018;19(2):108-19. doi: 10.1038/s41590-017-0022-x. PubMed PMID: 29348500; PubMed Central PMCID: PMC5854158.
12. Youn JI, Gabrilovich DI. The biology of myeloid-derived suppressor cells: the blessing and the curse of morphological and functional heterogeneity. Eur J Immunol. 2010;40(11):2969-75. doi: 10.1002/eji.201040895. PubMed PMID: 21061430; PubMed Central PMCID: PMC3277452.
13. Lang S, Bruderek K, Kaspar C, Hoing B, Kanaan O, Dominas N, et al. Clinical Relevance and Suppressive Capacity of Human Myeloid-Derived Suppressor Cell Subsets. Clin Cancer Res. 2018;24(19):4834-44. doi: 10.1158/1078-0432.CCR-17-3726. PubMed PMID: 29914893.
14. Raychaudhuri B, Rayman P, Huang P, Grabowski M, Hambardzumyan D, Finke JH, et al. Myeloid derived suppressor cell infiltration of murine and human gliomas is associated with reduction of tumor infiltrating lymphocytes. J Neurooncol. 2015;122(2):293-301. doi: 10.1007/s11060-015-1720-6. PubMed PMID: 25579983.
15. Wen X, Jeong S, Kim Y, Bae JM, Cho NY, Kim JH, et al. Improved results of LINE-1 methylation analysis in formalin-fixed, paraffin-embedded tissues with the application of a heating step during the DNA extraction process. Clin Epigenetics. 2017;9:1. Epub 2017/02/06. doi: 10.1186/s13148-016-0308-0. PubMed PMID: 28149329; PubMed Central PMCID: PMC5270344.
16. Bankhead P, Loughrey MB, Fernandez JA, Dombrowski Y, McArt DG, Dunne PD, et al. QuPath: Open source software for digital pathology image analysis. Sci Rep. 2017;7(1):16878. Epub 2017/12/06. doi: 10.1038/s41598-017-17204-5. PubMed PMID: 29203879; PubMed Central PMCID: PMC5715110.
17. Kamentsky L, Jones TR, Fraser A, Bray MA, Logan DJ, Madden KL, et al. Improved structure, function and compatibility for CellProfiler: modular high-throughput image analysis software. Bioinformatics. 2011;27(8):1179-80. Epub 2011/02/26. doi: 10.1093/bioinformatics/btr095. PubMed PMID: 21349861; PubMed Central PMCID: PMC3072555.
18. Nagaraj S, Schrum AG, Cho HI, Celis E, Gabrilovich DI.

Mechanism of T cell tolerance induced by myeloid-derived suppressor cells. J Immunol. 2010;184(6):3106-16. doi: 10.4049/jimmunol.0902661. PubMed PMID: 20142361; PubMed Central PMCID: PMC2832724.
19. Huang YK, Wang M, Sun Y, Di Costanzo N, Mitchell C, Achuthan A, et al. Macrophage spatial heterogeneity in gastric cancer defined by multiplex immunohistochemistry. Nat Commun. 2019;10(1):3928. doi: 10.1038/s41467-019-11788-4. PubMed PMID: 31477692; PubMed Central PMCID: PMC6718690.
20. Law AMK, Valdes-Mora F, Gallego-Ortega D. Myeloid-Derived Suppressor Cells as a Therapeutic Target for Cancer. Cells. 2020;9(3). doi: 10.3390/cells9030561. PubMed PMID: 32121014; PubMed Central PMCID: PMC7140518.
21. Veglia F, Sanseviero E, Gabrilovich DI. Myeloid-derived suppressor cells in the era of increasing myeloid cell diversity. Nat Rev Immunol. 2021. doi: 10.1038/s41577-020-00490-y. PubMed PMID: 33526920; PubMed Central PMCID: PMC7849958.
22. Alshetaiwi H, Pervolarakis N, McIntyre LL, Ma D, Nguyen Q, Rath JA, et al. Defining the emergence of myeloid-derived suppressor cells in breast cancer using single-cell transcriptomics. Sci Immunol. 2020;5(44). doi: 10.1126/sciimmunol.aay6017. PubMed PMID: 32086381; PubMed Central PMCID: PMC7219211.
23. Vayrynen JP, Haruki K, Vayrynen SA, Lau MC, Dias Costa A, Borowsky J, et al. Prognostic significance of myeloid immune cells and their spatial distribution in the colorectal cancer microenvironment. J Immunother Cancer. 2021;9(4). Epub 2021/05/02. doi: 10.1136/jitc-2020-002297. PubMed PMID: 33931472; PubMed Central PMCID: PMC8098931.

초록

서론: 골수 유래 억제 세포(MDSC)는 다양한 세포로 구성된 미분화된 골수성세포로 암을 비롯한 질병상태에서 관찰할 수 있다. MDSC는 암 미세환경에서 중요한 역할을 수행한다고 알려져 있지만 진행서 위암에서 MDSC의 구성과 임상적 특성과의 유의성에 대해서는 알려져 있지 않다

방법: 59명의 진행성 위암조직에서 채취한 검체가 사용되었다 Tissue microarray와 multiplex immunohistochemistry가 MDSC와 T 세포의 아형을 분석하는데 이용되었다. 임상적 특성 및 예후와의 관련성에 분석하였다.

결과: MDSC 중 PMN-MDSC가 가장 풍부하였으며 M-MDSC가 그 뒤를 이었다. CIMP-음성 위암은 MDSC가 풍부한 경우에도 상대적으로 T 세포의 밀도나 낮은 반면 CIMP-양성 위암은 MDSC와 T세포 양쪽 모두 높게 나타났다. PD-L1 발현은 MDSC 중에서는 M-MDSC가 PD-1 발현은 T 세포 중에서 CD8양성 T세포에서 높게 나타났다. 세가지 MDSC 모두 다른 골수성세포에 비해 암세포에 가깝게 위치하고 있었으며 T세포 중에서는 CD8양성 T세포가 가장 암세포와 가까웠다.

결론: 이 실험을 통해 MDSC가 진행성 위암에서 독특한 특성을 지니면서 특이한 위치에 자리매김한다는 것을 밝힐 수 있었다. 이 같은 MDSC 만의 특성은 면역치료를 비롯한 암을 치료함에 있어서 매우 중요하게 작용할 것이다.

주요어: 골수유래면역억제세포, 진행성 위암, 종양미세환경,
다중면역화학염색법, 예후, 면역체계

학번: 2012-21737